

LONG ROLLS GENERATED BY NATURAL CONVECTION IN AN INCLINED, RECTANGULAR ENCLOSURE

HIROYUKI OZOE and KEIICHI FUJII

Okayama University, Tsushima, Okayama, 700 Japan

and

NOAM LIOR and STUART W. CHURCHILL*

University of Pennsylvania, Philadelphia, PA 19104, U.S.A.

(Received 23 February 1982 and in revised form 18 January 1983)

Abstract—The three-dimensional velocity and temperature fields, and in turn the average Nusselt number and representative streaklines were computed by a finite-difference method for a cellular element with a length-to-height ratio of 7 and several postulated width-to-height ratios near unity in a rectangular enclosure heated from below, perfectly insulated on the lateral surfaces, and inclined about the long dimension. Calculations were carried out for $Ra = 4000$, $Pr = 10$ and a single grid spacing (non-uniform in the long dimension) for cells with dragless lateral boundaries and for those with one dragless and one rigid. Computations such as these have previously been utilized to develop a simple, theoretically based method for the prediction of Nu in horizontal enclosures of arbitrary aspect ratios. Further calculations are necessary to support such a method of prediction for inclined enclosures and to define its limits of applicability.

NOMENCLATURE

f	arbitrary function
g	acceleration due to gravity [$m\ s^{-2}$]
H	distance between heated and cooled surfaces [m]
k	thermal conductivity [$W\ m^{-1}\ K^{-1}$]
L	width of cell [m]
l	dimensionless width of cell, L/H
Nu	average Nusselt number, $qH/k(T_h - T_c)$
Pr	Prandtl number, ν/α
q	average heat flux density [$W\ m^{-2}$]
Ra	Rayleigh number, $g\beta(T_h - T_c)H^3/\alpha\nu$
T	temperature [K]
T_c	temperature of cold surface [K]
T_h	temperature of hot surface [K]
t	time [s]
u	velocity component in x -direction [$m\ s^{-1}$]
U	dimensionless velocity component in x -direction, uH/α
V	velocity vector [$m\ s^{-1}$]
v	velocity component in y -direction [$m\ s^{-1}$]
V	dimensionless velocity component in y -direction, vH/α
w	velocity component in z -direction [$m\ s^{-1}$]
W	dimensionless velocity component in z -direction, wH/α
x	coordinate in shorter horizontal dimension of enclosure [m]
X	dimensionless coordinate in x -direction, x/H
\bar{X}	transformed dimensionless coordinate in x -direction [see equation (9)]
y	coordinate in longer horizontal dimension of enclosure [m]

Y	dimensionless coordinate in y -direction, y/H
z	distance from cold plate [m]
Z	dimensionless coordinate in z -direction, z/H

Greek symbols

α	thermal diffusivity [$m^2\ s^{-1}$]
β	volumetric coefficient of expansion with temperature [K^{-1}]
θ	angle of inclination of heated surface from horizontal [rad]
ν	kinematic viscosity [$m^2\ s^{-1}$]
τ	dimensionless time, $t\alpha/H^2$
Φ	dimensionless temperature, $(2T - T_h - T_c)/2(T_h - T_c)$
ψ	dimensionless vector potential [defined by equation (5)]
ψ_i	i -component of dimensionless vector potential
Ω	dimensionless vorticity vector [defined by equation (4)]
Ω_i	i -component of dimensionless vorticity vector

Subscripts

c	center of cell ($X = 3.5$, $Y = 0.5l$, $Z = 0.5$)
i	index; x , y and z

1. INTRODUCTION

NATURAL convection in inclined rectangular enclosures of low aspect ratio, with heating from below, is of practical interest in a number of applications including solar collectors and double glazed windows. This behavior has, therefore, received extensive study experimentally. However, as indicated below, theoretical results are quite limited in scope.

*To whom correspondence should be addressed at the Department of Chemical Engineering.

As observed by Ozoe *et al.* [1] for air and silicone oil and by Oertel [2] for nitrogen and silicone oil, at the Rayleigh number of this investigation (4000), the stable flow pattern for low angles of inclination about the longer dimension as an axis is a series of stationary rolls with their axes in the upslope, as shown in Fig. 1. As shown photographically by Ozoe *et al.* [3], each of these rolls is confined to a rectangular volume, hereafter designated as a cell, whose dimensions do not change with inclination, i.e. each fluid particle remains within the cell. It is this observation that makes possible the model and calculations presented herein.

At some critical angle, a transition occurs from these multiple cells to a single circulation up the heated and down the cooled surface. According to the theory of Hart [4] and the experiments of Hollands and Konicek [5], the critical angle for $Ra = 4000$ and a nearly infinite layer of fluid is $65\pi/180$ rad. As discussed by Clever and Busse [6], Ruth *et al.* [7], Oertel [2] and others, transitions to unstable (turbulent) convection may also occur as a complex function of Ra , Pr , inclination and the aspect ratios.

Ozoe *et al.* [1, 8–11] and Arnold *et al.* [12] have shown experimentally, and Ozoe *et al.* [10, 11, 13] theoretically, that for channels (finite in 2-dim.) and boxes (finite in 3-dim.) the Nusselt number goes through a minimum, then a maximum, and finally decreases to unity, as the angle of inclination about the longer horizontal dimension as an axis is increased from 0 to π rad. The inclinations for the minimum and maximum in the Nusselt number were found by Ozoe *et al.* [1] to be independent of the Rayleigh number and the major aspect ratio over the range of their experiments (for which $Ra \cos \theta$ always exceeded the critical Rayleigh number for no inclination) but to be a strong function of the minor aspect ratio. The minimum in the Nusselt number was found from photographs [3] and computations [10, 13, 14] to be associated with the transition from a series of rolls with their long dimension in the upslope to a single circulation with its axis parallel to the longer dimension. The rolls in the series (before transition) were each found to be composed of two symmetrical half-rolls. Fluid particles are restricted to one of these half-rolls. As the

inclination increases the half-rolls become more and more distorted, and the curved plane of separation of their particle-paths becomes increasingly oblique to the axis of the cell. Transition occurs when this plane of separation crosses the diagonal plane of the cell. The maximum in the Nusselt number appears to occur when the upper edge of the enclosure passes above the diagonally opposite lower edge (the axis of inclination), thus providing the greatest vertical path for the fluid. Ayyaswamy and Catton [15] showed that the solution of Gill [16] for the boundary layer regime of a vertical channel ($\theta = \pi/2$ rad) could be adapted for an inclined channel in the single-roll regime. Catton *et al.* [17] subsequently used the Galerkin method to derive an approximate solution for this same regime. Ozoe *et al.* [8, 9] developed finite-difference solutions for the single-roll regime of inclined $1 \times \infty \times 1$ and $2 \times \infty \times 1$ channels.

The fluid motion is 3-dim. in the multiple-roll regime of inclined channels and for all conditions in boxes, thereby severely handicapping theoretical analysis. Three-dimensional solutions for inclined enclosures, prior to this paper, are apparently restricted to the finite-difference solutions of Ozoe *et al.* for a $1 \times \infty \times 1$ channel [13], a $2 \times \infty \times 1$ rectangular channel [14], and a $1 \times 2 \times 1$ box [10, 11]. Oertel [2] has noted that the influence of those surfaces which produce three-dimensionality in a horizontal enclosure dies away within a distance approximately equal to the height of the enclosure. Therefore, the error in the overall Nusselt number due to the neglect of three-dimensionality decreases as the two aspect ratios increase. However, he further indicates that effect of three-dimensionality is more pervasive with inclination.

This paper presents the first detailed study of the fluid motion within a *long* cellular region (herein called a cell) in the multiple-roll regime of a finite enclosure inclined about its longer dimension. Results were obtained by the finite-difference solution of a 3-dim. model for the velocity and temperature fields. The rate of heat transfer was in turn computed from the latter. The calculations were restricted by reasons of economy to the representative conditions of $Ra = 4000$, $Pr = 10$, and a cell length-to-height ratio of 7. Cells with both free-free and rigid-free lateral boundaries were considered, corresponding to central and edge cells, respectively, in a finite enclosure. The only significant idealization in the model is the postulate of a fixed, known cell width.

The results of this basic study are presumed to be applicable to finite-enclosures insofar as this mode of circulation prevails and insofar as the width of the roll cells can be postulated. Ozoe *et al.* [18] have recently utilized corresponding results for a horizontal enclosure to predict the overall Nusselt number without empiricism other than for interpolation. A similar general method of prediction for enclosures inclined about their long dimension as an axis will require lengthy computations for additional Rayleigh numbers, Prandtl numbers, aspect ratios and grid sizes.

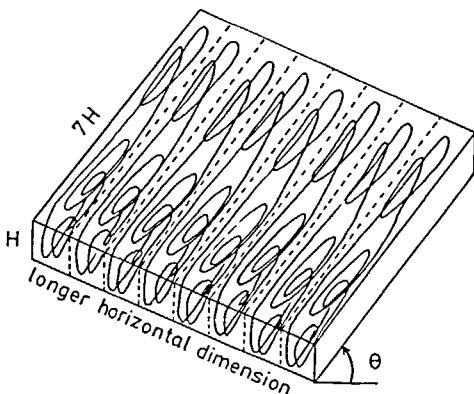


FIG. 1. Sketch of roll cells in an inclined enclosure.

In addition, the range of conditions in which the postulated mode of circulation occurs must be defined experimentally. The simplicity and utility of such a method of prediction would appear to justify this additional work, despite its high cost.

2. CELL WIDTH

The applicability of the calculations in this paper to enclosures depends on the advance postulate of a known cell width for each Rayleigh number, Prandtl number and pair of aspect ratios. The state of knowledge on this subject will therefore first be examined.

The width-to-height ratio of the roll cells in an infinite layer of low-Prandtl-number fluid, confined between rigid, horizontal, isothermal surfaces and heated from below is known to increase from unity as the Rayleigh number increases above its critical value. Koschmieder [19] provides a thorough discussion of these data. However, Dubois and Bergé [20] recently showed experimentally that for a large-Prandtl-number fluid the cell width remains equal to the height for Rayleigh numbers up to ten times the critical value. All early theoretical analyses based on 2-dim. models [19] predicted a decrease in cell width with Rayleigh number. Eventually, however, Lipps and Somerville [21], using a 3-dim. transient model, obtained cell widths in agreement with the experimental observations, and hence concluded that the increase in roll-cell width is a 3-dimensional, transient process even though the steady motion is 2-dim.

Oertel [11] carried out a theoretical and experimental study of cell width for rectangular boxes. Because of the lateral confinement, a change in cell width requires a change in the number of roll cells and hence is an essentially discrete process. He observed experimentally that for nitrogen ($Pr = 0.7$) the number of roll cells in a $4 \times 10 \times 1$ box changed from 10 to 9 at $Ra = 2300$, to 8 at 5650 and to 7 at 8900. Transition to turbulence then began at $Ra = 11\,300$. On the other hand, for silicone oil ($Pr = 1780$), the number remained at 10 up to $Ra = 12\,000$. This result was generally confirmed by his finite-difference calculations, although that formulation, because of an artificially imposed symmetry, permitted only an even number of roll cells. He concluded from experiments with both nitrogen gas and silicone oil that the same general behavior occurs in inclined boxes, but did not provide quantitative evidence.

The computed and experimental streaklines of Oertel indicate that the two cells adjacent to the lateral walls are somewhat narrower than the eight intermediate ones, which are essentially uniform in width. However, Samuels and Churchill [22], using 2-dim. finite-difference calculations found that the cells adjacent to the walls were slightly wider than the central one in a $3 \times \infty \times 1$ channel.

Ozoe *et al.* [3], in a photographic study of roll cells in glycerol ($Pr = 3000$) at $Ra = 12\,000$ in a $2 \times 12 \times 1$ box,

found that the number of cells remained constant at 12 up to the angle of transition at about $7\pi/180$ rad. The width of the bounding cells, which may have been influenced by the finite conductivity of the side walls, did not differ significantly from the intermediate ones, and was in some cases greater and in others less.

From the above results, it is concluded that the cell width-to-height ratio in a finite enclosure should be nearly unity for the conditions of this study ($Ra = 4000$, $Pr = 10$ and a length-to-height ratio of 7). Furthermore, this ratio would not be expected to change significantly for other Rayleigh numbers from the critical value up to at least 12 000, for larger Pr , and for other length-to-height ratios. This ratio might increase stepwise with Ra for smaller Pr . Therefore, the basic calculations were carried out for a ratio of cell width-to-height ratio of unity, but test calculations were carried out for a range of cell width-to-height ratios to determine the sensitivity of the circulation and the Nusselt number to this ratio.

For the multiple-cell regime the division of the circulation into two rigid-free cells and a number of identical free-free cells is physically justifiable insofar as the correct width-to-height ratios of these two types of cell can be specified. For the single circulation which occurs at large inclinations, such a division has no physical counterpart. However, this procedure is justifiable mathematically insofar as the effect of the drag of the lateral boundaries is confined to a distance of less than one height unit from the wall.

3. MATHEMATICAL MODEL AND PROCEDURE

The 3-dim. model, finite-difference approximation, and process of solution previously used by Ozoe *et al.* [13] for a 2×1 rectangular channel were adapted for the $7H \times L \times H$ cell illustrated in Fig. 2. The final form of the model in terms of the vector potential and vorticity, and expressed in dimensionless variables is

$$\nabla \cdot \psi = 0, \tag{1}$$

$$\frac{D\Omega}{D\tau} - (\Omega \cdot \nabla)\mathbf{V} = RaPr \begin{pmatrix} -\frac{\partial\Phi}{\partial y} \cos \theta \\ \frac{\partial\Phi}{\partial z} \sin \theta + \frac{\partial\Phi}{\partial x} \cos \theta \\ -\frac{\partial\Phi}{\partial y} \sin \theta \end{pmatrix} + Pr\nabla^2\Omega \tag{2}$$

and

$$\frac{D\Phi}{D\tau} = \nabla^2\Phi \tag{3}$$

where

$$\Omega = \nabla \times \mathbf{V} = -\nabla^2\psi \tag{4}$$

and

$$\mathbf{V} = \nabla \times \psi. \tag{5}$$

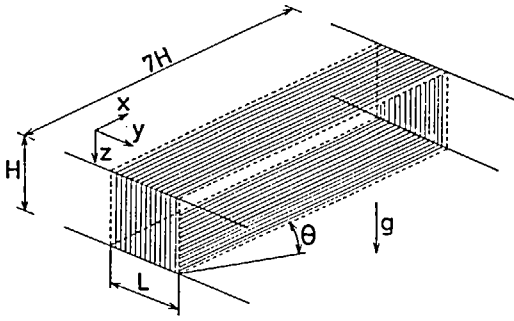


FIG. 2. Schematic of cellular region in a rectangular enclosure with T_c at $z = 0$ and T_h at $z = H$.

The boundary conditions for the cell with dragless boundaries at $Y = 0$ and l , and adiabatic surfaces at $X = 0, 7$ are

$$\frac{\partial \psi_x}{\partial X} = \psi_y = \psi_z = \Omega_x = 0, \Omega_y = -\frac{\partial W}{\partial X},$$

$$\Omega_z = \frac{\partial V}{\partial X}, \frac{\partial \Phi}{\partial X} = 0 \text{ at } X = 0, 7, \quad (6)$$

$$\psi_x = \frac{\partial \psi_y}{\partial Y} = \psi_z = \frac{\partial U}{\partial Y} = \frac{\partial W}{\partial Y} = \Omega_x = \Omega_z = 0;$$

$$\frac{\partial \Omega_y}{\partial Y} = \frac{\partial \Phi}{\partial Y} = 0 \text{ at } Y = 0, l, \quad (7)$$

$$\psi_x = \psi_y = \frac{\partial \psi_z}{\partial Z} = \Omega_z = 0, \Omega_x = -\frac{\partial V}{\partial Z},$$

$$\Omega_y = \frac{\partial U}{\partial Z}, \Phi = \mp 0.5 \text{ at } Z = 0, 1. \quad (8)$$

For a cell at the edge of the enclosure the boundary condition at $Y = 0$ was replaced with the analog of the one for $X = 0$. The lateral walls of the enclosure were thus also postulated to be adiabatic.

For the finite-difference approximation a uniform grid spacing of 0.1 was used in the Y and Z directions, and 10 equal spaces in

$$\bar{X} = 1.512771829 \ln(1 + 2.60317127X) \quad (9)$$

for $0 \leq X \leq 3.5$, and 10 symmetrically located spaces for $3.5 \leq X \leq 7.0$, as illustrated in Fig. 3.

The derivatives of an arbitrary function of X can be approximated in terms of \bar{X} as

$$\left(\frac{\partial f}{\partial X}\right)_i = \frac{\partial f}{\partial \bar{X}} \frac{\partial \bar{X}}{\partial X} \cong \frac{f(\bar{X}_{i+1}) - f(\bar{X}_{i-1})}{2\Delta \bar{X}} \left(\frac{\partial \bar{X}}{\partial X}\right) \quad (10)$$

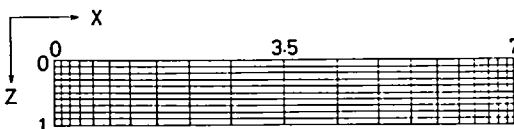


FIG. 3. Grid array for finite difference calculations.

and

$$\left(\frac{\partial^2 f}{\partial X^2}\right)_i = \frac{\partial f}{\partial \bar{X}} \frac{\partial^2 \bar{X}}{\partial X^2} + \frac{\partial^2 f}{\partial \bar{X}^2} \left(\frac{\partial \bar{X}}{\partial X}\right)^2$$

$$\cong \frac{f(\bar{X}_{i+1}) - f(\bar{X}_{i-1})}{2\Delta \bar{X}} \left(\frac{\partial^2 \bar{X}}{\partial X^2}\right) + \frac{f(\bar{X}_{i+1}) + f(\bar{X}_{i-1}) - 2f(\bar{X}_i)}{(\Delta \bar{X})^2} \left(\frac{\partial \bar{X}}{\partial X}\right)^2. \quad (11)$$

Alternatively, the derivatives can be approximated by a Taylor series expansion in terms of X, Y and Z as

$$\left(\frac{\partial f}{\partial X}\right)_i = \left(\frac{X_i - X_{i-1}}{X_{i+1} - X_i}\right) \left(\frac{f_{i+1} - f_i}{X_{i+1} - X_{i-1}}\right) + \left(\frac{X_{i+1} - X_i}{X_i - X_{i-1}}\right) \left(\frac{f_i - f_{i-1}}{X_{i+1} - X_{i-1}}\right) \quad (12)$$

and

$$\left(\frac{\partial^2 f}{\partial X^2}\right)_i = \frac{2f_{i+1}}{(X_{i+1} - X_i)(X_{i+1} - X_{i-1})} - \frac{2f_i}{(X_i - X_{i-1})(X_{i+1} - X_i)} + \frac{2f_{i-1}}{(X_i - X_{i-1})(X_{i+1} - X_{i-1})}. \quad (13)$$

Test calculations with $f = X^2, X^3$ and e^x revealed that equations (10) and (11) provide a less accurate representation than equations (12) and (13). Hence the latter were used.

The dimensionless temperature and three components of the vorticity, vector potential and velocity were computed from the finite-difference model. Representative streaklines were in turn calculated from the velocity field and the average Nusselt number from the temperature field.

4. RESULTS

4.1. Dependence of circulation and Nusselt number on cell width

In the multiple-roll regime the cell is aligned with the shorter horizontal dimension. Thus a dimensionless cell length (length-to-height ratio) of 7.0 implies an enclosure with an equal or greater dimensionless width (width-to-height ratio). Finite-difference calculations for such a dimensionless width are precluded by the amount of computation which would be required by the associated number of grid points. The restriction of attention to a single cell greatly reduces the computations, but imposes the arbitrary postulate of a cell width. The dependence of the fluid motion and heat transfer on the postulate was therefore first investigated, and for simplicity, for no inclination.

The average Nusselt number, Nu ; the absolute value of the dimensionless X -component of the vector potential at the center of the roll, $|\psi_x|_c$; and the volumetric averages of U^2, V^2, W^2 and $U^2 + V^2 + W^2$

are plotted versus the postulated dimensionless cell width in Fig. 4(a) for drag-free lateral boundaries. The square of the components of the velocity and their sum are proportional to the corresponding kinetic energies. The average Nusselt number and the volumetric average of the total kinetic energy, which is a measure of the overall strength of the circulation, are seen to have their maximum value at $l \cong 1$. The individual volumetric averages of V^2 and W^2 are seen to cross over at this point, while U^2 is negligible for all l . The quantity $|\psi_x|_c$ which is a measure of the strength of the circulation for a roll with its axis in the x -direction peaks at $l \cong 1.25$.

Figure 4(b) is the comparable plot for a cell, adjacent to the side wall of the enclosure, with one rigid and one dragless lateral boundary. In this case the average Nusselt number peaks at $l \cong 1.1$, the volumetric average kinetic energy at ~ 1.2 and $|\psi_x|_c$ at ~ 1.4 . The

volumetric averages of U^2 and W^2 cross over at $l = 1.03$, and again U^2 is negligible for all l .

This test is obviously indecisive, although the predominance of evidence indicates the most stable dimensionless cell width is in the range of 1.0 to 1.1, which is in accord with prior observations and calculations. The calculations for inclined cells were therefore limited to $l = 1.0$ and 1.1.

4.2. Mean Nusselt number across an inclined cell

The computed mean Nusselt numbers for $7 \times 1 \times 1$ cells with free-free and rigid-free lateral boundaries are plotted versus the angle of inclination in Fig. 5. The Nusselt number is seen to be lower, as expected, for the rigid-free cell. Just as for the $1 \times 1 \times 1$ and $2 \times 1 \times 1$ cells previously studied [10, 11, 14], a decrease to a minimum value (at the point of transition from multiple roll cells to a single one) followed by an increase to a maximum value and a decrease to unity is to be observed as the inclination increases from 0 to π rad.

The minimum and the maximum occur at essentially the same angles for free-free and the rigid-free lateral boundaries. The indicated angle of $50\pi/180$ rad for the minimum is in good agreement with the prediction of $49\pi/180$ rad by the empirical correlation of Ozoe *et al.* [1] and the indicated maximum angle of $\sim 87\pi/180$ rad with the theoretical prediction of $\tan^{-1}(7) = 82\pi/180$ rad by Churchill and Ozoe [23].

The average Nusselt numbers calculated for a dimensionless cell width of 1.1 did not differ significantly from those calculated for 1.0, as indicated in Fig. 5 by the solid triangles for a free-rigid cell. Hence the postulate of a cell width would not be expected to influence greatly the predictions for a finite enclosure.

4.3. Volumetric-average kinetic energy of an inclined cell

The open symbols in Fig. 6 indicate the variation of the volumetric-average kinetic energy and the contributions of its three components with inclination for a free-free cell. These values are for $l = 1.0$. Representative values (solid and half-solid symbols) are

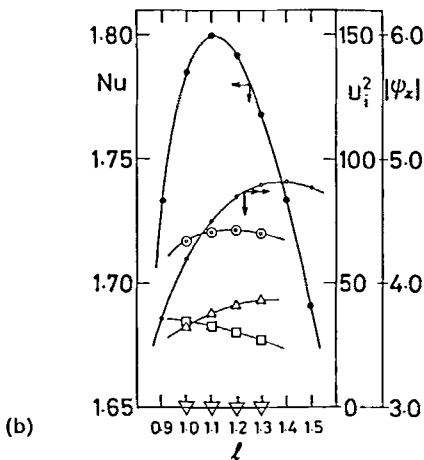
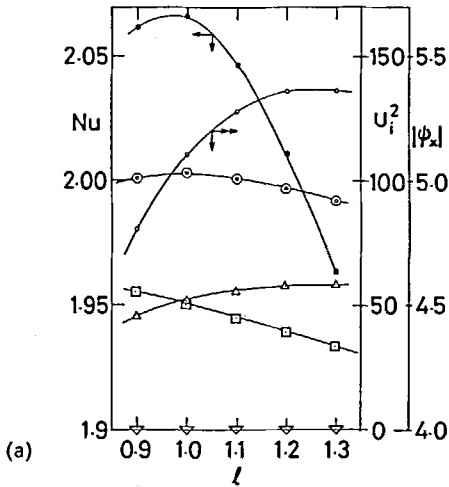


FIG. 4. Effect of roll width on Nu ; the volumetric average of U^2 , V^2 , W^2 and $U^2 + V^2 + W^2$; and $|\psi_x|_c$.

—●— Nu , —○— $|\psi_x|_c$, —○— $U^2 + V^2 + W^2$, —▽— U^2 , —△— V^2 , —□— W^2 . (a) Dragless lateral boundaries for cell (free-free). (b) One dragless and one rigid lateral boundary for cell (free-rigid).

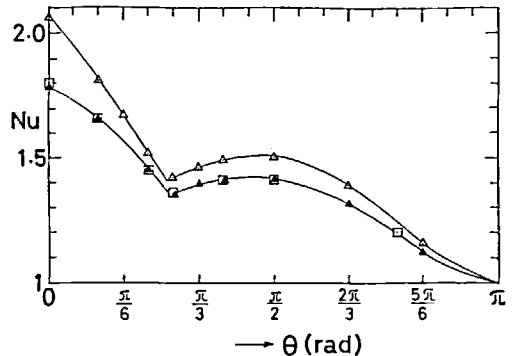


FIG. 5. Effect of inclination on average Nusselt number of cell. —△— free-free boundaries; $l = 1$, —▲— free-rigid boundaries; $l = 1$, —□— free-rigid boundaries; $l = 1.1$.

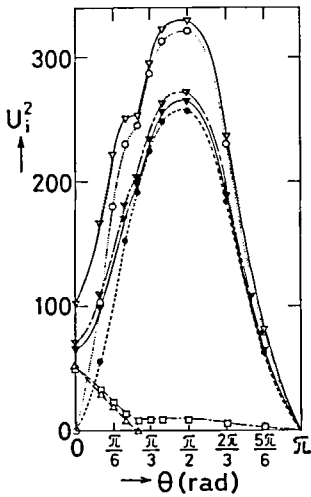


FIG. 6. Effect of inclination on volumetric average of squared velocities:

	free-free, $l = 1$	free-rigid, $l = 1$	free-rigid, $l = 1.1$
$U^2 + V^2 + W^2$	-▽-	▼	-▽-
U^2	·○·	·●·	
V^2	-△--		
W^2	-□--		

included for a free-rigid cell (with $l = 1.0$ and 1.1 , respectively).

Inclination is seen to produce a rapid increase in U^2 from near zero, and a rapid decrease in V^2 and W^2 . For the free-free boundary condition, V^2 is properly zero beyond the point of transition to a single 2-dim. circulation path: W^2 is relatively small beyond this point but has a finite value owing to the reversal in the direction of circulation at the ends of the cell. A noticeable break occurs in U^2 and in $U^2 + V^2 + W^2$ at the point of transition. The maximum in these latter two quantities occurs at the same angle as for Nu . All of these values are higher for the free-free cell than for the free-rigid one, and all are slightly higher for $l = 1.1$ than for 1.0 for the free-rigid cell.

4.4. Vector potential at the center of an inclined cell

The three components of the dimensionless vector potential at the center of the cell ($X = 3.5$, $Y = 0.5l$, $Z = 0.5$) are plotted versus the angle of inclination in Fig. 7. ψ_x and ψ_z are properly zero at all locations (although only the value at the center of the cell is shown) for a free-free cell at inclinations beyond the point of transition. For the free-rigid cell these two quantities are zero at the center but have finite values elsewhere owing to the three-dimensionality imposed by the drag of the lateral wall.

4.5. Streaklines in an inclined cell

The character of the circulation is more clearly revealed by the representative streaklines in Figs. 8-18. Each streakline represents the transient, cyclic motion of a fluid particle in a steady state flow field. Traces of

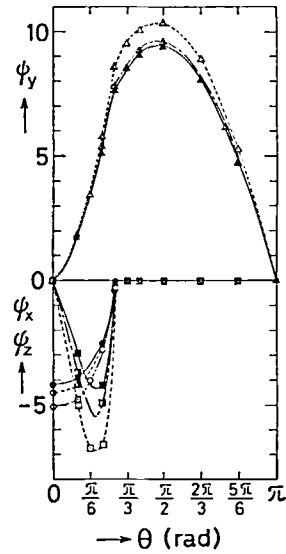


FIG. 7. Effect of inclination on components of vector potential at center of cell:

	free-free, $l = 1$	free-rigid, $l = 1$	free-rigid, $l = 1.1$
ψ_x	-○-	●	●
ψ_y	-△-	▼	▼
ψ_z	-□-	■	■

streaklines are shown for the free-free cell at inclinations of 0 , $20\pi/180$, $30\pi/180$, and $40\pi/180$ rad in Figs. 8-11, and a perspective view for the same inclinations plus $90\pi/180$ rad in Fig. 12.

The streakline for no inclination reveals a spiral movement near the ends of the cell. This calculation was stopped after 3000 time-steps with $\Delta\tau = 0.002$ to conserve computer time. If the calculation had been continued, a coaxial return spiral to the initial point would have been produced. It can be inferred from this plot that the effect of the drag of the end walls is essentially confined to one dimensionless length, i.e. all streaklines in the central region would be nearly 2-dim. in an x -plane. The circulation is composed of two antisymmetrical, half rolls in corresponding halves of the cell itself. It has been confirmed experimentally [24] that all fluid particles are confined to one or the other of these half cells. For no inclination the plane of separation of the half cells is the central x -plane.

For inclinations of $20\pi/180$, $30\pi/180$ and $40\pi/180$, the streaklines are seen in Figs. 9-12 to become increasingly oblique and complex. The curved plane of separation of the two half cells gradually approaches the diagonal plane of the cell. The axis of the roll is curved but remains in the midplane parallel to the heated surface at $30\pi/180$ rad. However, for $40\pi/180$ rad, the single streakline which is shown extends over the length of the cell and the circulation pattern is no longer a simple roll. For inclinations greater than $50\pi/180$ rad, the streaklines are 2-dim. in a y -plane. This pattern is maintained for all higher inclinations, as illustrated in Fig. 12(e) for $90\pi/180$ rad.

Corresponding streaklines for a free-rigid cell with

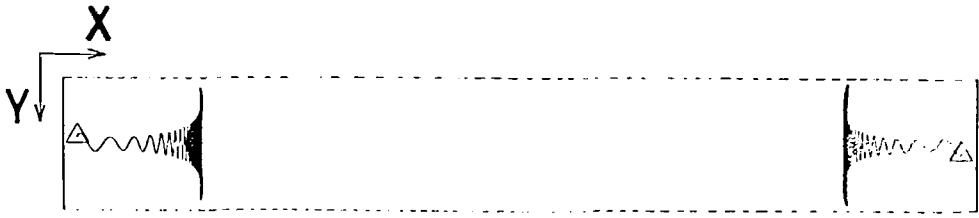


FIG. 8. Top view of streaklines for no inclination in a free-free cell with $l = 1$. Δ -Starting points $(0.1, 0.45, 0.45)$ and $(6.9, 0.55, 0.55)$ $\tau = 6$, $\Delta\tau = 0.002$.

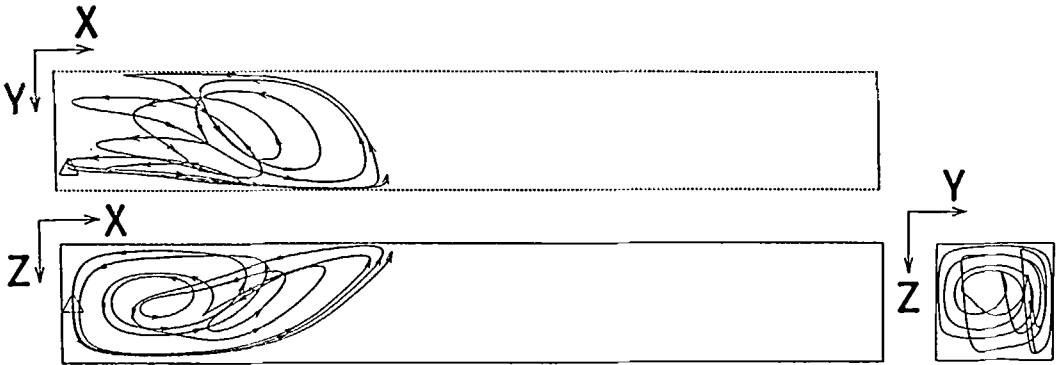


FIG. 9. Traces of streaklines for $\theta = 20\pi/180$ rad in a free-free cell with $l = 1$. Δ -Starting point $(0.1, 0.8, 0.5)$ $\tau = 3$, $\Delta\tau = 0.002$.

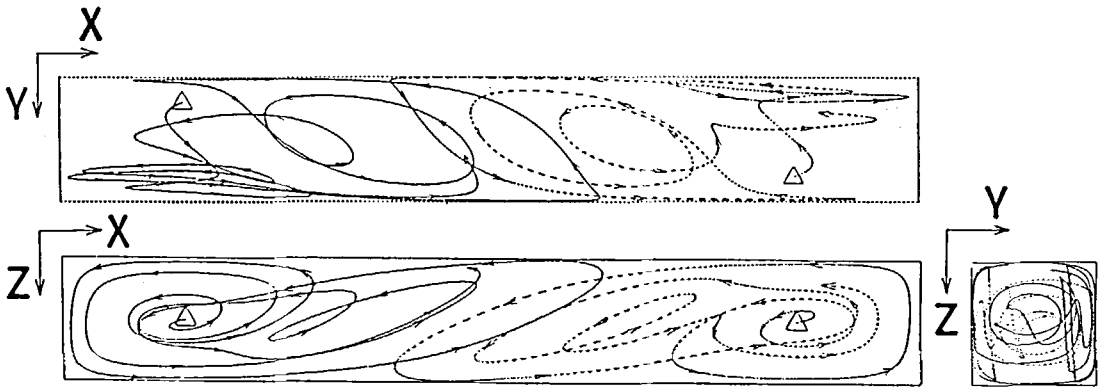


FIG. 10. Traces of streaklines for $\theta = 30\pi/180$ rad in a free-free cell with $l = 1$. Δ -Starting points $(1.0, 0.2, 0.5)$ and $(6.0, 0.8, 0.5)$ $\tau = 3$, $\Delta\tau = 0.002$.

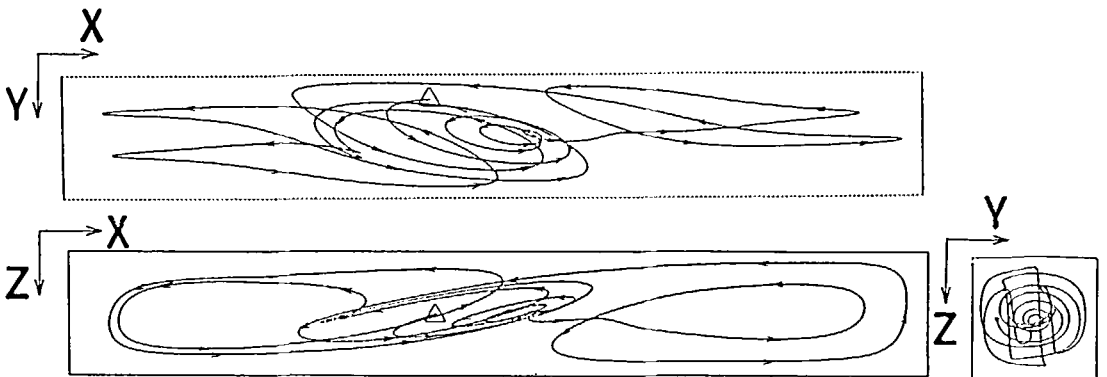


FIG. 11. Traces of streaklines for $\theta = 40\pi/180$ rad in a free-free cell with $l = 1$. Δ -Starting point $(3.0, 0.2, 0.5)$ $\tau = 3$, $\Delta\tau = 0.002$.

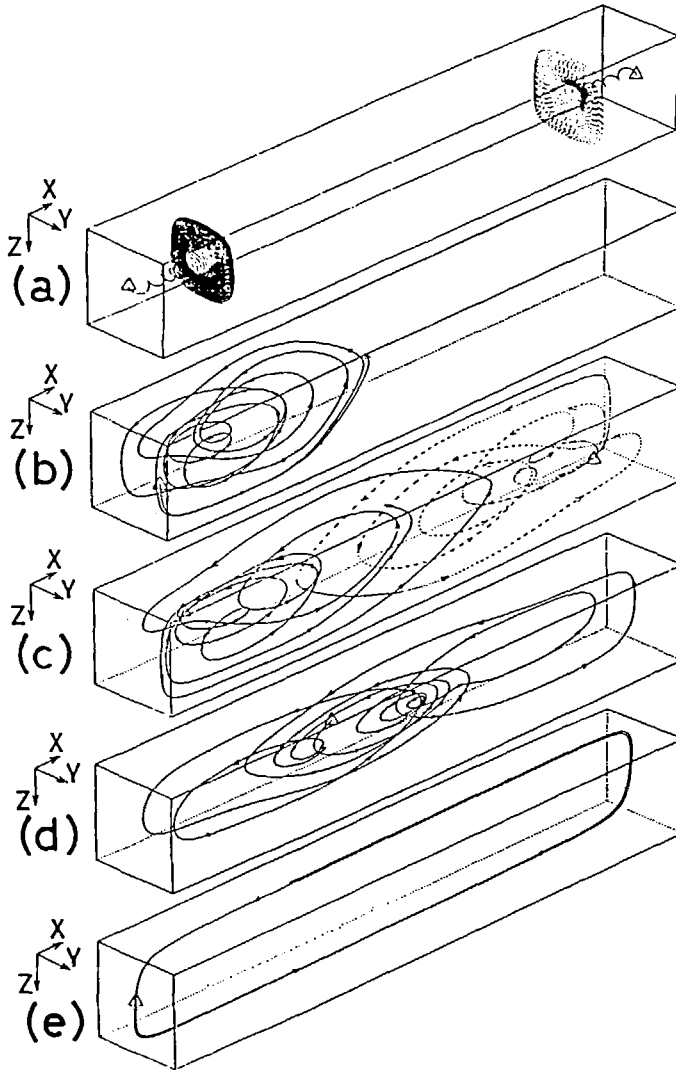


FIG. 12. Perspective view of streaklines for various inclinations for a free-free cell with $l = 1$. Δ -Starting points (0.1, 0.5, 0.5) for $\theta = 90\pi/180$ rad, otherwise same as before. Eye point (-100, 100, -70). (a) $\theta = 0$ rad. (b) $\theta = 20\pi/180$ rad. (c) $\theta = 30\pi/180$ rad. (d) $\theta = 40\pi/180$ rad. (e) $\theta = 90\pi/180$ rad.

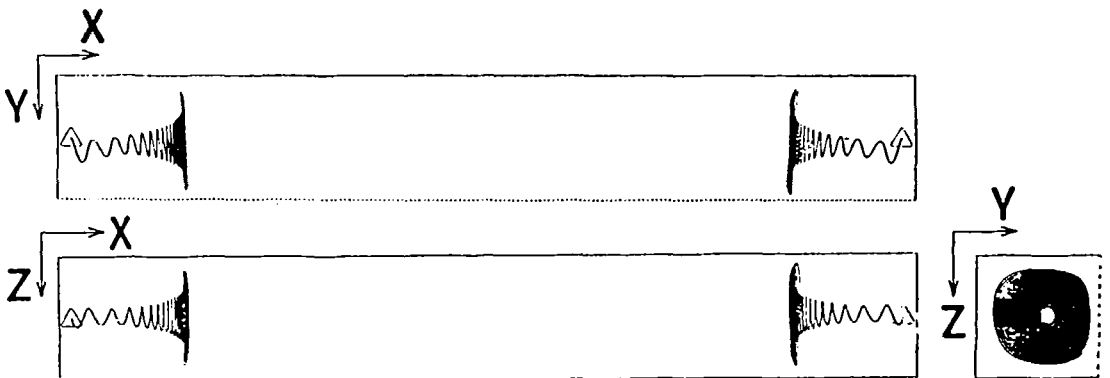


FIG. 13. Traces of streaklines for no inclination of free-rigid cell with $l = 1$. Δ -Starting points (0.1, 0.5, 0.5) and (6.9, 0.5, 0.5) $\tau = 4$, $\Delta\tau = 0.002$.

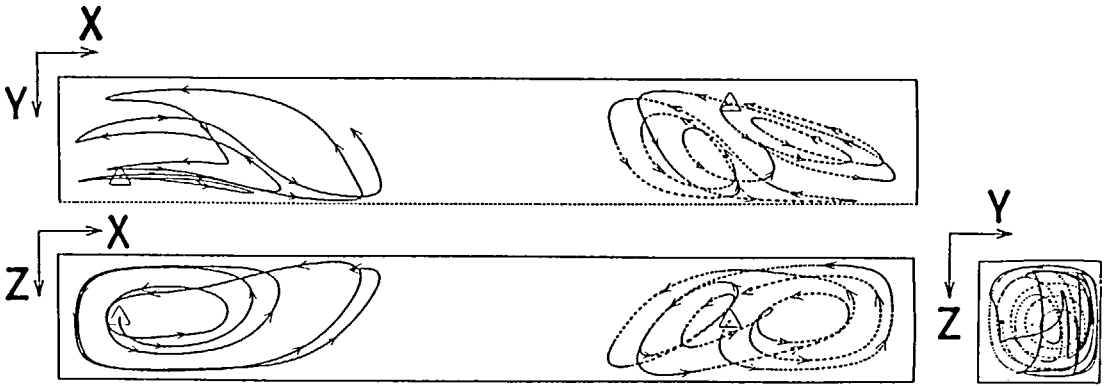


FIG. 14. Traces of streaklines for $\theta = 20\pi/180$ rad in free-rigid cell with $l = 1$. Δ -Starting points (0.5, 0.8, 0.5) and (5.5, 0.2 and 0.5) $\tau = 2$, $\Delta\tau = 0.02$.

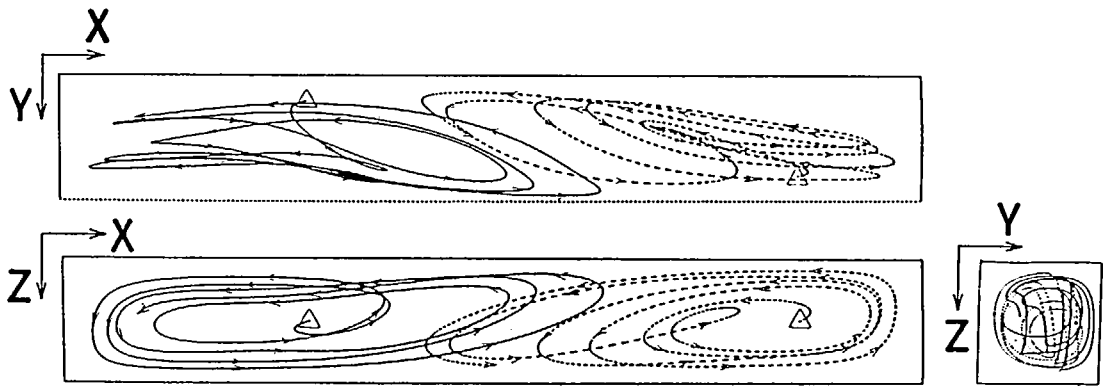


FIG. 15. Traces of streaklines for $\theta = 40\pi/180$ rad in free-rigid cell with $l = 1$. Δ -Starting points (2.0, 0.2, 0.5) and (6.0, 0.8, 0.5) $\tau = 2$, $\Delta\tau = 0.002$.

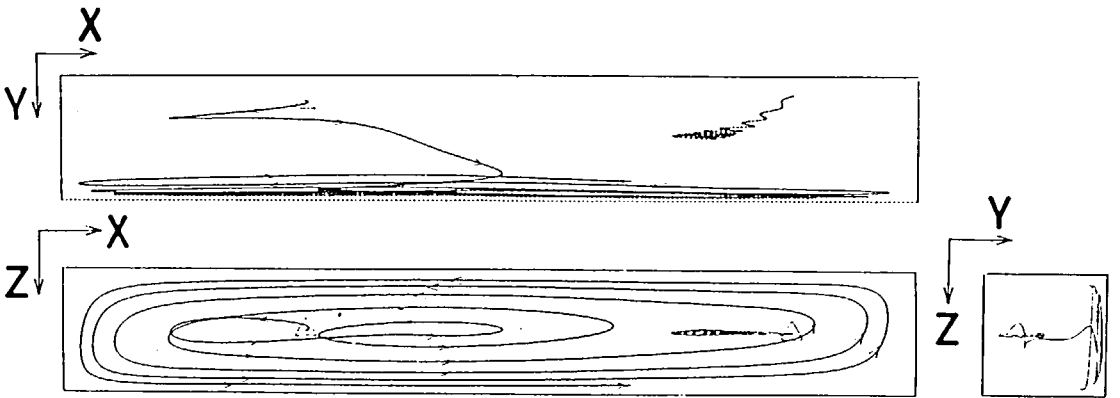


FIG. 16. Traces of streaklines for $\theta = 50\pi/180$ rad in free-rigid cell with $l = 1$. Δ -Starting points (2.0, 0.2, 0.5) and (6.0, 0.15, 0.5) $\tau = 4$, $\Delta\tau = 0.002$.

$l = 1$ are illustrated in Figs. 13–18. For no inclination the circulation is similar to that for the free-free cell but is slightly eccentric. At $40\pi/180$ rad, the particle paths do not extend as far as for the free-free cell. At $50\pi/180$ rad, the illustrated particle path near the free boundary is nearly 2-dim., but the second particle path reveals a nearly stagnant region in the central core, accounting for the minimum in the Nusselt

number. The circulation is seen to be quasi-2-dim. at $90\pi/180$ rad. The nearly stagnant central core is responsible for the lower Nusselt number relative to the horizontal case. The same interpretation is applicable to the free-free cell.

The streaklines computed for $l = 1.1$ were not found to differ significantly from those for $l = 1.0$, and hence are not reproduced here.

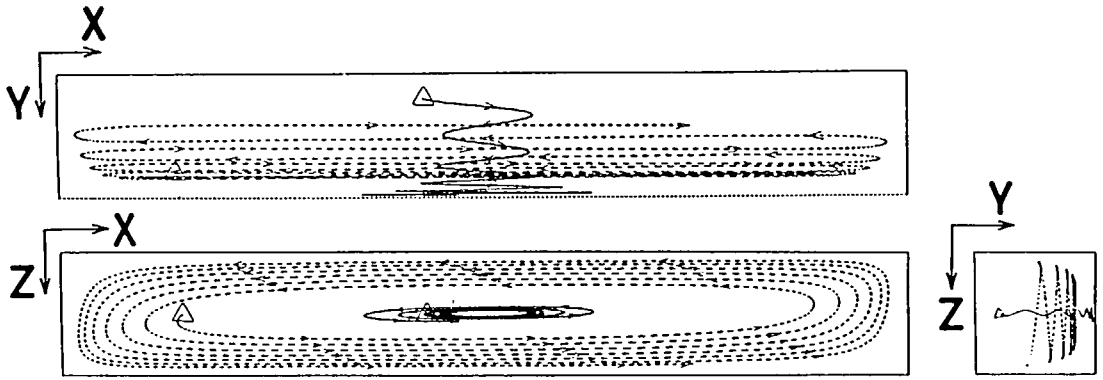


FIG. 17. Traces of streaklines for $\theta = 90\pi/180$ rad in free-rigid cell with $l = 1$. Δ -Starting points $(3.0, 0.2, 0.5)$ and $(1.0, 0.8, 0.5)$ $\tau = 4, \Delta\tau = 0.02$.

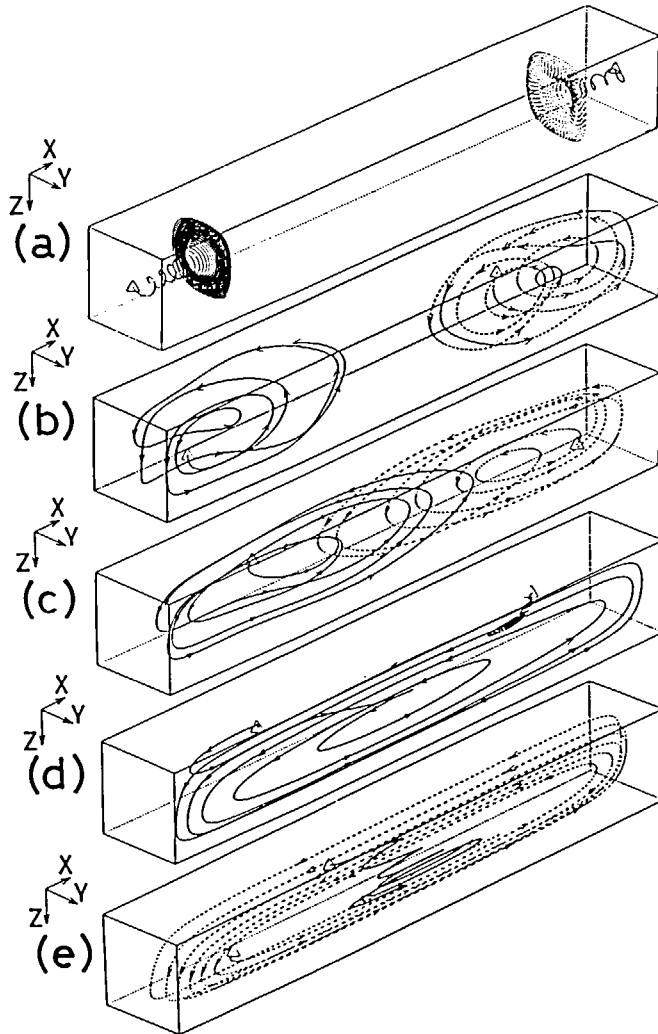


FIG. 18. Perspective view of streaklines for various inclinations of free-rigid cell with $l = 1$. Δ -Starting points are the same as before. Eye point $(-100, 100, -70)$. (a) $\theta = 0$ rad. (b) $\theta = 20\pi/180$ rad. (c) $\theta = 40\pi/180$ rad. (d) $\theta = 50\pi/180$ rad. (e) $\theta = 90\pi/180$ rad.

5. SUMMARY AND CONCLUSIONS

This paper presents the first theoretical results for the 3-dim. fluid motion and for the rate of heat transfer in the multiple-cell regime of rectangular enclosures of large but finite dimensions, inclined about the longer dimension as an axis.

The postulate of a known, fixed cell width and the use of a staggered grid in the longer dimension made solution by finite-differences feasible for this geometry. The persistence of such fixed, essentially square cells has previously been confirmed experimentally.

Calculations were carried out for two dragless lateral boundaries, corresponding to a cell in the central region of the enclosure, and for one dragless and one rigid lateral boundary, corresponding to a cell next to one of the lateral walls of the enclosure. This division into only two types of cells is justifiable physically for the multiple-roll regime, insofar as the effect of the drag of the lateral walls does not extend beyond one height unit. This latter postulate has been confirmed experimentally.

The calculations were limited to $Ra = 4000$ and $Pr = 10$ but are presumed to be quantitatively applicable for larger Pr and qualitatively for smaller Pr , and for larger Ra in the laminar regime. However, an unstable (turbulent) motion may occur for some yet undefined ranges of Pr and Ra .

The calculations are limited to a single finite grid spacing but are presumed on the basis of prior calculations for related behavior to be in only slight error due to truncation. Empirical extrapolation of the Nusselt number for this grid spacing to zero grid size may be possible, but extensive further calculations would still be necessary.

The strength of the flow pattern is characterized by plots of the volumetric average kinetic energy and by the component of the vector potential in the direction of the long dimension of the cell. The angle of inclination for transition from the regime of multiple rolls to a single circulation is clearly identifiable from these plots.

The results of this investigation are applicable for the theoretical prediction, without any empiricism, of heat transfer in finite rectangular enclosures, but are incomplete in that respect, results for other grid-spacings, cell lengths, Prandtl numbers and Rayleigh numbers being necessary. In addition experimental measurements are necessary to define the conditions under which this type of stable cellular motion occurs.

Acknowledgements—Partial support of this work was provided by the U.S. Department of Energy Solar Heating and Cooling R&D Branch through Contract EM-78-04-5365. The participation of Professor H. Ozoe in the work at the University of Pennsylvania was made possible through the Joint U.S.-Japan Cooperative Research Program co-sponsored by the Japan Society for the Promotion of Science and the U.S. National Science Foundation. Partial support for the work in Japan was provided by a Grant in Aid for Scientific Research on Special Research Projects on Energy Problems from the Ministry of Education, Japan (No. 56040063).

REFERENCES

1. H. Ozoe, H. Sayama and S. W. Churchill, Natural convection in an inclined rectangular channel at various aspect ratios and angles—experimental measurements, *Int. J. Heat Mass Transfer* **18**, 1425–1431 (1975).
2. H. Oertel, Jr., Three-dimensional convection within rectangular boxes, *ASME HTD* **8**, 11–16 (1980); *Thermische Zellularkonvektion*, Habilitationsschrift, Universität Karlsruhe (1979).
3. H. Ozoe, H. Sayama and S. W. Churchill, Natural convection patterns in a long inclined rectangular box heated from below. Part I. Three-directional photography, *Int. J. Heat Mass Transfer* **20**, 123–129 (1977).
4. J. E. Hart, Stability of the flow in a differentially heated inclined box, *J. Fluid Mech.* **47**, 547–576 (1971).
5. K. G. T. Hollands and L. Konicek, Experimental study of the stability of differentially inclined air layers, *Int. J. Heat Mass Transfer* **16**, 1467–1476 (1973).
6. R. M. Clever and F. H. Busse, Instability of longitudinal convection rolls in an inclined layer, *J. Fluid Mech.* **81**, 101–127 (1977).
7. D. W. Ruth, K. G. T. Hollands and G. D. Raithby, On free convection experiments in inclined air layers heated from below, *J. Fluid Mech.* **96**, 461–479 (1980).
8. H. Ozoe, K. Yamamoto, H. Sayama and S. W. Churchill, Natural convection in an inclined rectangular channel heated on one side and cooled on the opposing side, *Int. J. Heat Mass Transfer* **17**, 1209–1217 (1974).
9. H. Ozoe, H. Sayama and S. W. Churchill, Natural convection in an inclined square channel, *Int. J. Heat Mass Transfer* **17**, 401–406 (1974).
10. H. Ozoe, S. W. Churchill, T. Okamoto and H. Sayama, Three-dimensional natural convection in inclined rectangular enclosures, *Proc. PACHEC-II*, Vol. 1, pp. 24–31. A.I.Ch.E., New York (1977).
11. H. Ozoe, S. W. Churchill, T. Okamoto and H. Sayama, Natural convection in doubly inclined rectangular boxes, *Proc. 6th Int. Heat Transfer Conf.*, Toronto, Vol. 2, NC-19, pp. 293–298. Hemisphere, Washington DC (1978).
12. J. N. Arnold, I. Catton and D. K. Edwards, Experimental investigation of natural convection in inclined rectangular regions of differing aspect ratios, *J. Heat Transfer* **98**, 67–71 (1976).
13. H. Ozoe, K. Yamamoto and S. W. Churchill, Three-dimensional numerical analysis of natural convection in an inclined channel with a square cross section, *A.I.Ch.E.J.* **25**, 709–716 (1979).
14. H. Ozoe, H. Sayama and S. W. Churchill, Natural convection patterns in a long rectangular box heated from below, Part II. Three-dimensional numerical results, *Int. J. Heat Mass Transfer* **20**, 131–139 (1977).
15. P. Ayyaswamy and I. Catton, The boundary layer regions for natural convection in a differentially heated, tilted rectangular cavity, *J. Heat Transfer* **95**, 543–545 (1973).
16. A. E. Gill, The boundary-layer regime for convection in a rectangular cavity, *J. Fluid Mech.* **26**, 515–526 (1966).
17. I. Catton, P. S. Ayyaswamy and R. M. Clever, Natural convection in a finite, rectangular slot arbitrarily oriented with respect to the gravity vector, *Int. J. Heat Mass Transfer* **17**, 173–184 (1974).
18. H. Ozoe, K. Fujii, S. W. Churchill and N. Lior, A theoretically based correlation for natural convection in horizontal rectangular enclosures heated from below with arbitrary aspect ratios, *Proc. 7th Int. Heat Transfer Conf.*, Munich, Vol. 2, NC23, pp. 257–268 (1982).
19. E. L. Koschmieder, Bénard convection, *Adv. Chem. Phys.* **26**, 177–211 (1974).
20. M. Dubois, and P. Bergé, Experimental study of the velocity field in Rayleigh–Bénard convection, *J. Fluid Mech.* **85**, 641–653 (1978).
21. F. B. Lipps and R. C. J. Somerville, Dynamics of variable wavelength in finite-amplitude Bénard convection, *Physics Fluids* **14**, 759–765 (1971).

22. M. R. Samuels and S. W. Churchill, Stability of a fluid in a rectangular region heated from below, *A.I.Ch.E. J.* **11**, 77–85 (1967).
23. S. W. Churchill and H. Ozoe, The description and prediction of natural convection in inclined rectangular enclosures, in preparation.
24. H. Ozoe, N. Sato and S. W. Churchill, Experimental confirmation of the three-dimensional helical streaklines previously computed for natural convection in inclined rectangular enclosures, *Kagaku Kogaku Ronbunshu* **5**, 19–25 (1979) (in Japanese); English transl., *Int. Chem. Engng* **19**, 454–462 (1979).

ROULEAUX ALLONGES PAR CONVECTION NATURELLE DANS UNE ENCEINTE INCLINEE ET RECTANGULAIRE

Résumé—Les champs tridimensionnels de vitesse et de température, et par suite le nombre de Nusselt moyen et la ligne de courant sont calculés par une méthode aux différences finies pour une cellule avec un rapport longueur-hauteur égal à 7 et plusieurs rapports largeur-hauteur proche de l'unité dans une enceinte rectangulaire chauffée à la base, parfaitement isolée sur les faces latérales et inclinée par la grande dimension. Des calculs sont faits pour $Ra = 4000$, $Pr = 10$ et un espacement unique (non uniforme dans la grande dimension) pour des cellules avec des frontières sans trainée et pour d'autres avec une frontière sans trainée et l'autre rigide. Des calculs tels que ceux-ci ont été précédemment utilisés pour développer une méthode simple théorique pour la prévision de Nu dans des enceintes horizontales avec des rapports de forme arbitraires. D'autres calculs sont nécessaires pour appuyer cette méthode dans le cas des enceintes inclinées et pour définir ses limites d'application.

LANGE WIRBELWALZEN, DIE DURCH NATÜRLICHE KONVEKTION IN EINEM GENEIGTEN, RECHTECKIGEN HOHLRAUM ENTSTEHEN

Zusammenfassung—Mit Hilfe eines finiten Differenzen-Verfahrens wurde für ein zellenartiges Element das dreidimensionale Geschwindigkeits- und Temperaturfeld und daraus die mittlere Nusselt-Zahl und repräsentative Stromlinien berechnet. Für den rechteckigen Hohlraum werden ein Längen/Höhen-Verhältnis von 7 und verschiedene Breiten/Höhen-Verhältnisse nahe 1 angenommen. Der Raum wird von unten beheizt, ist an den Seitenwänden ideal isoliert und in Längsrichtung geneigt. Die Berechnungen wurden für $Ra = 4000$ und $Pr = 10$ mit einem ungleichmäßigen Gitter ausgeführt, und zwar für Zellen mit reibungsfreien seitlichen Begrenzungen und für solche, bei denen die eine zeitliche Begrenzung reibungsfrei und die andere fest ist. Ähnliche Berechnungen sind bereits verwendet worden, um ein einfaches, theoretisch begründetes Verfahren zur Berechnung der Nu -Zahl in waagerechten Hohlräumen mit beliebigen Seitenverhältnissen zu entwickeln. Um ein derartiges Berechnungsverfahren auf geneigte Hohlräume anwenden zu können, und die Grenzen seiner Anwendbarkeit zu bestimmen, sind weitere Berechnungen erforderlich.

ДЛИННЫЕ ВАЛЫ, ОБРАЗУЮЩИЕСЯ ПРИ ЕСТЕСТВЕННОЙ КОНВЕКЦИИ В НАКЛОННЫХ ПРЯМОУГОЛЬНЫХ ПОЛОСТЯХ

Аннотация—Конечно-разностным методом рассчитаны трехмерные поля скорости и температуры, а также среднее значение числа Нуссельта и характерная структура течения для ячейки с отношением длины к высоте, равным 7, и несколькими отношениями ширины к высоте, близкими к единице, находящейся в нагреваемой снизу прямоугольной наклонной полости с теплоизолированными боковыми поверхностями. Расчеты выполнялись для значений $Ra = 4000$ и $Pr = 10$ на одной и той же сетке (неравномерной вдоль длины полости) для ячеек со свободными боковыми границами и для ячеек с одной свободной и одной твердой боковыми границами. Подобные расчеты уже производились ранее для разработки простого теоретического метода расчета числа Nu в горизонтальных полостях с произвольными отношениями сторон. Дальнейшие расчеты необходимы для обобщения метода на случай наклонных полостей и для определения границ его применимости.